Journal of Applied Sciences and Nanotechnology

Journal homepage: jasn.uotechnology.edu.iq

Performance Comparison of Plasmonic Sensors via Ion Reduction and KOH Methods

Ruqaya Abdulkareem Shlaga*, Alwan M. Alwan, Mohammed S. Mohammed

Department of Applied Sciences, University of Technology - Iraq, Iraq

A R T I C L E I N F O

Article history:
Received: August, 24, 2024
Accepted: May, 02, 2025
Available online: June, 10, 2025

Keywords:
CIPRO antibiotics,
CIPRO antibiotics,
Pre-etching ion reduction,
KOH method

Corresponding Author:
Ruqaya Abdulkareem Shlaga
ruqaya12322@gmail.com

A B S T R A C T

In this work, several types of plasmonic sensors were prepared by different methods (ion reduction method and wet-chemical KOH route) to detect the ultralow anti-CIPRO concentration using AgNPs/PSi SERS-active substrate with AgNPs concentration. The process was optimized to be very effective in detecting CIPRO and to have a high amplification factor (EF). For the deposition of AgNPs with a concentration of 5×10^{-3} M and the maximum density of hotspot areas, a nanocrystalline silicon sample prepared by the KOH method and an ion reduction technique before etching was used. We tested an AgNPs/PSi SERS substrate, which showed better performance in detecting the CIPRO antibiotic over a range of doses (10^{-7}-10^{-13} M). XRD, EDX, FESEM and SERS were used to analyze the PSi samples and the AgNP/PSi chemical sensors. The results of the AgNPs/PSi SERS substrates from both methods showed that the ion reduction process was more effective in detecting the CIPRO antibiotics at their lowest concentrations. It was found that the highest EF at salt concentrations of 5×10^{-3}M was 6.3×10^{12} for the pre-etching method, compared with 7.78×10^{10} for the KOH method under the same conditions. The results showed that the proposed AgNPs/PSi SERS substrate is an effective method to find CIPRO even at low concentrations, and that CIPRO was localized approximately near the surface. This approach is considered a revolutionary work that has the potential to modify the plasmonic properties of metallic NPs for SERS applications.

https://doi.org/10.53293/jasn.2025.7488.1317, Department of Applied Sciences, University of Technology - Iraq.

1. Introduction

Antibiotics are active pharmaceutical ingredients that changed medicine in the twentieth century. They have revolutionized the treatment of many diseases and helped to save countless lives. Due to their remarkable efficacy against a wide range of infectious diseases, these pharmaceutical agents have significantly improved the longevity and well-being of humans and animals [1].

Ciprofloxacin, a fluoroquinolone antibiotic with a broad spectrum of activity, is suitable for the prevention and treatment of infectious diseases in humans and animals [2]. It is effective against a broad spectrum of Gram-negative and Gram-positive bacteria [3-5]. It inhibits type II DNA gyrase and topoisomerase IV, two essential

enzymes for DNA segregation in bacteria, and subsequently reduces cell division [6, 7], leading to fragmentation of genomic DNA. Due to the irregular misuse of antibiotics, antibiotic residues accumulate in animal feed [8], and in the environment [7, 9-12].

Antibiotics can enter the environment through a variety of pathways, e.g. through the infiltration of wastewater from humans and other animals, through leaks in landfills, through effluents from sewage treatment plants and through agricultural runoff that bypasses these systems [13]. Conventional wastewater treatment methods are known to leave pharmaceuticals in wastewater [14], and the spread of bacteria resistant to antibiotics poses a major health risk to humans and other animals [15-20]. To prevent the spread of antibiotics in water sources, the identification of antibiotics is crucial [21]. Surface-enhanced Raman scattering (SERS) based on metal nanoparticles has become the gold standard for the detection of pesticides, antibiotics and other environmental pollutants.

To detect extremely low concentrations of CIPRO, it is crucial to identify the highest peak in the SERS spectrum. The hot-spot density and the presence of localized surface plasmons (LSP) have a direct influence on the intensity of the Raman signal [22, 23]. Manipulation of PSi morphology is one approach to overcome these limitations. This can be achieved by increasing the density of the hot spots and using PSi as a template for silver or gold nanoparticles (AgNPs and AuNPs). The active substrate for SERS can be either AuNPs/PSi or AgNPs/PSi. With increasing EF, the metallic nanoparticles aggregate, resulting in a higher number of hot spots [24, 25]. In this study, innovative techniques to modify the plasmonic properties and morphology of AgNPs by utilizing the thermal effects of a laser beam were presented. In addition, a new method was developed to prepare a highly efficient AgNPs/PSi SERS-active substrate for the detection of extremely low concentrations of the drug CIPRO in the range of 10^{-7} - 10^{-13} M [26].

2. Experimental Procedure

An n-type silicon wafer was employed, which had a crystallite orientation of 100, a thickness of around 514 µm, and a resistivity of around 10 Ω.cm. Si wafers were weighed after being sliced into squares with a (1×1) cm^2 area, washed with a hydrofluoric: ethanol combination (1:10) to remove the SiO_2 coating, and then measured. Finally, it is stored in methanol-filled plastic containers before and after etching to prevent oxidation.

The PSi structures were synthesized in a two-step procedure. First, wet-chemical texturization was performed by immersing the silicon samples in a 2 M KOH solution for 30 min under laser illumination (wavelength ≈ 405 nm, intensity ≈ 350 mW/cm²), which facilitated surface modification by anisotropic etching. Subsequently, the textured Si substrates were immersed in a 5×10^{-3} M $AgNO_3$ solution for 10 minutes to deposit AgNPs on the nanostructured surfaces. The entire laser-assisted KOH etching process is shown schematically in **Fig. 1.**

The second is the pre-etching ion reduction process. This procedure started by being the standard pre-etching of the Si substrate and the formation of AgNPs. The substrates were immersed in a hydrofluoric acid solution at a 15% M concentration for 12 hours at room temperature with typical daylight light irradiation and local heating process for both the surface of crystalline and AgNPs by laser intensity of about 350 mW/cm^2 for a period of 30 min. The goal of this process was to make more silver ion reduction centers available for making silver nanoparticles by increasing the number of dangling bonds (SiH_x, where x = 1, 2, 3, etc.) on the surface of the crystalline silicon. Using this approach, a layer of AgNPs on the surface is generated by reducing silver ions through dangling bonds on the silicon substrate. To accomplish this operation, the crystalline Si substrates were dipped into a 5×10^{-3}M concentration of silver nitrate solution, as shown in **Fig. 2**.

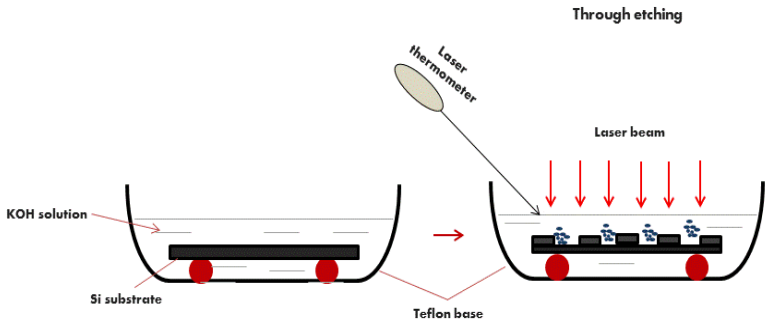

Figure 1: A schematic KOH method that has been laser improved to change the Si surface.

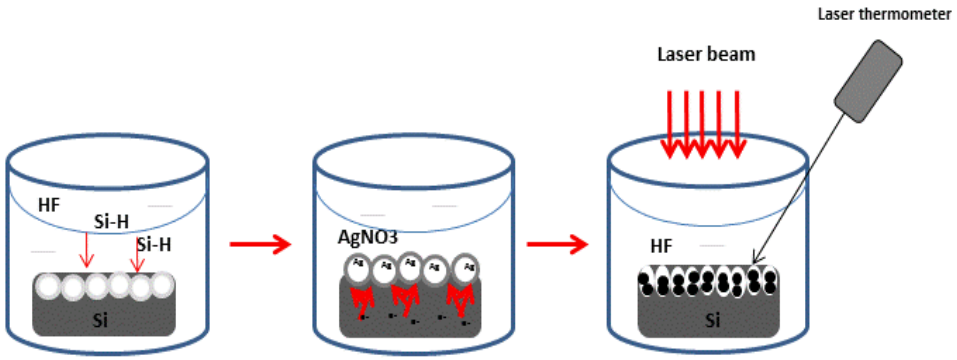

Figure 2: A schematic of the creation of Si nanostructures utilizing an ion reduction technique with laser treatment.

3. Results and Discussion

FESEM picture illustrates the deposited AgNPs upon the surface is shown in **Fig. 3a, b** at a fixed (5×10^{-3} M) concentration and of the immersion time and laser intensity of about 350 mW/cm^2 with a wavelength of 405 nm for the KOH method and pre-etching ion reduction process. The NPs that are deposited form a layer without identifiable shapes, which is due to the density of dangling bonds SiH_x, x = 1. These bonds are more concentrated on the top surface after the porous silicon has been prepared and irradiated with an intensity of 350 mW/cm^2. From **Fig. 3a**, the presence of nanoparticles enhances the visibility of the porosity, where these nanoparticles primarily accumulate along the pore edges with a large size due to the ionic feature of the Ag particles, which implies that they cannot exist as individual atoms because of the sample's complete coverage and the presence of the atoms inside the pores, the single atoms would be drawn together to form particles made up of groups of atoms by the van der Waals mutual attraction force. While the Ag nanoparticles appeared well-formed, on the other hand, the porosity was distinctly visible with a high porous density and the presence of nanoparticles in small sizes, as shown in **Fig. 3b**. The examination images and calculation of the nanoparticle density on the PSi surface of the sample prepared by the ion reduction process showed that it has a higher percentage of NPs than the one prepared by the wet chemical KOH method (9×10^{12} and 5×10^{9}, respectively).

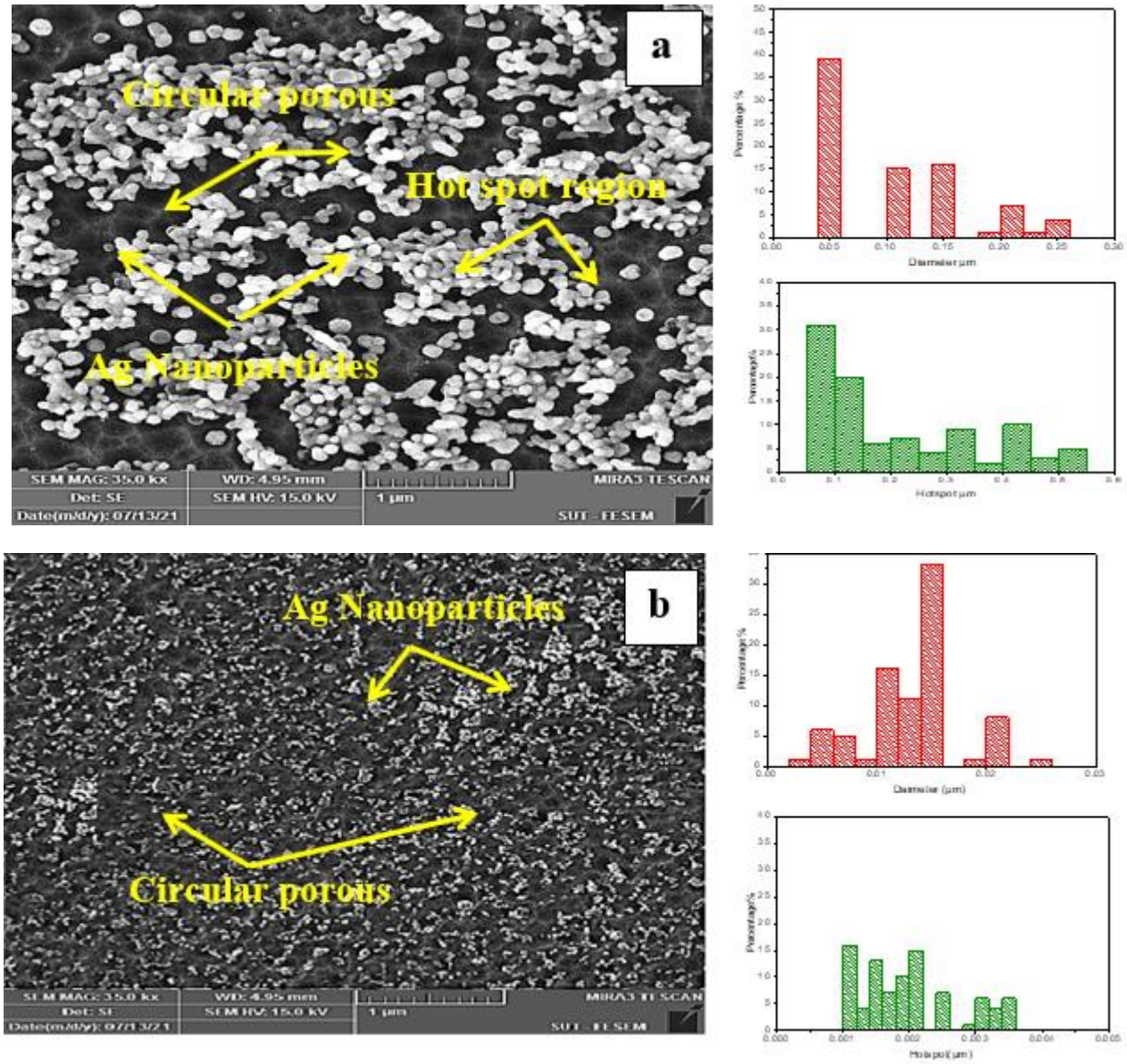

Figure 3: FESEM images and hotspot vacancy histograms of PSi prepared with 3500 mW/cm² laser and 10^{-3} M $AgNO_3$ via (a) KOH method and (b) ion reduction.

Based on the histogram, the size of Ag nanoparticles varied as displayed in **Fig. 3a, b**, the AgNP size varied from 39 nm to 290 nm for the sample prepared by the KOH method, while the pre-etching in the reduction process, the AgNPs' size varied from 4 nm to 25 nm. For the sample for KOH, the hotspot vacancy histogram of AgNPs ranged from 50 nm to 560 nm, while for the pre-etching ion reduction process, the hotspot vacancies varied from 1 nm to 3.8 nm.

The EDX spectra of the AgNPs deposition onto the Si substrate have been influenced via spectra for samples prepared by two methods: the KOH method and the pre-etching ion reduction process at a fixed concentration for AgNPs, time, and laser intensity, as shown in **Fig.4a, b**. These spectra showed a significant increase in the density of Ag and Si above the surface. The intensity of the Ag peak increased with the concentration of silver during preparation due to the increase in the nucleation site on the upper surface of Si. This explains the prominent AgNPs peak in the presence of KOH.

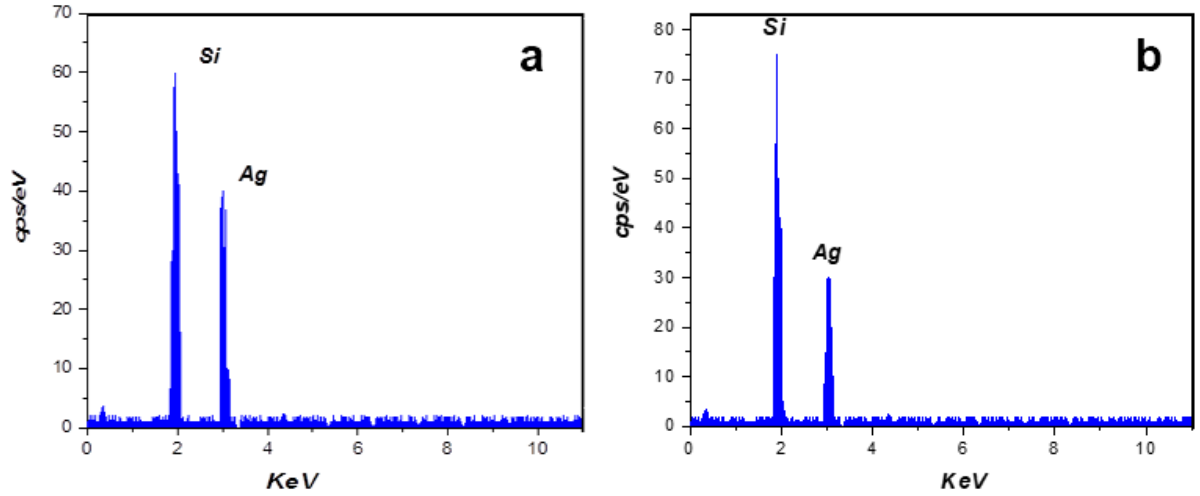

Figure 4: EDS measurement of AgNPs/Psi structures in a laser intensity of 3500 mW/cm^2 and 5×10^{-3}M of AgNPs concentrations: (a) KOH method and (b) pre-etching ion reduction process.

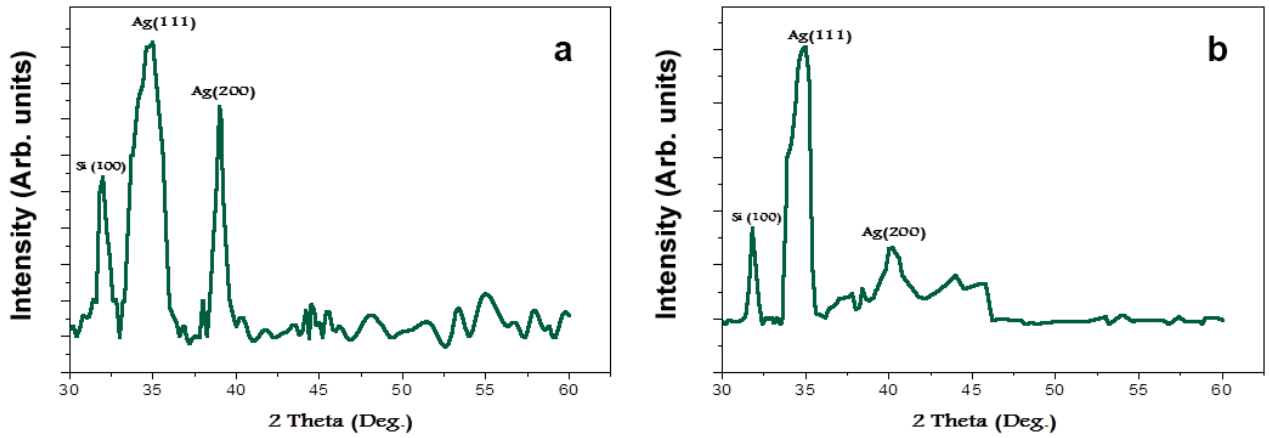

Figure 5: XRD patterns of AgNPs and Si nanocrystallites formed under different illumination conditions. Si peaks near 2θ ≈ 33.4° confirm (100) crystallinity, while AgNPs exhibit distinct Bragg reflections.

According to the data presented in **Table 1** for the KOH method and ion reduction process, the substrate exhibits a grain size value of approximately 4.759 nm in the (111) plane for pre-etching ion reduction, while for the KOH method, the grain size value is approximately 7.80nm. On the other hand, the substrate AgNPs exhibit a higher specific surface area (SSA) of approximately 120.191 m^2/g, whereas the lower value of about 73.28 m^2/g is for the substrate prepared by the KOH method. The deposited AgNPs grains size was determined using Scherer's formula and XRD peak expansion [27-34]. **Eq. (1)** calculates the SSA, one of the most significant metrics for characterization [35]:

$$SSA = \frac{6000}{\kappa \times Grain\ size} \quad (1)$$

Where, κ the density constant of silver (10.49 g/cm^3). For plasmonic NPs of different concentrations, **Table 1** shows the values of FWHM and grain size of AgNPs, and SSA.

Table 1: The FWHM, grains size, and SSA values of AgNPs for KOH and pre-etching ion reduction process.

Methods	Peaks	FWHM (Deg.)	Grain size (nm)	SSA (m^2/g)
Pre-etching Ion reduction process	111	1.767	4.759	120.191
KOH method		1.12	7.80	73.28

The FWHM of the XRD peaks is broadened with a laser light source by an etching process. The presence of tiny interatomic space modifications of the fabricated AgNPs on Si nanocrystallites causes the lowest deflection of the Bragg reflection peaks. The FWHM increases with decreasing size of the fabricated nanoparticles. Consequently, the diameters of the Si nanocrystallites change during the etching process, which affects the nanoparticles produced.

The performance of the AgNPs/PSi SERS sensor was evaluated based on different concentrations of antibiotics on nanostructure substrates. The obtained result shows that the Raman intensity of the CIPRO antibiotics has very shallow peaks even at AgNPs concentrations of about 5×10^{-3} M without illumination in the KOH process, while for the ion reduction process substrates, the peaks become higher than KOH as shown in **Fig. 6**. This is attributed to the presence of small-sized AgNPs, which are distinctly visible in the pores of the structure. **Fig. 7a, b** depict the Raman scattering spectra of antibiotics absorbed by AgNPs/PSi SERS active substrate at varied concentrations of about 10^{-7}-10^{-13} M, with stronger bonds at 1401 and 1600 cm^{-1} this is attributed to carboxylate group's (C-C) stretching bonds that interacted with the AgNPs surface [36].

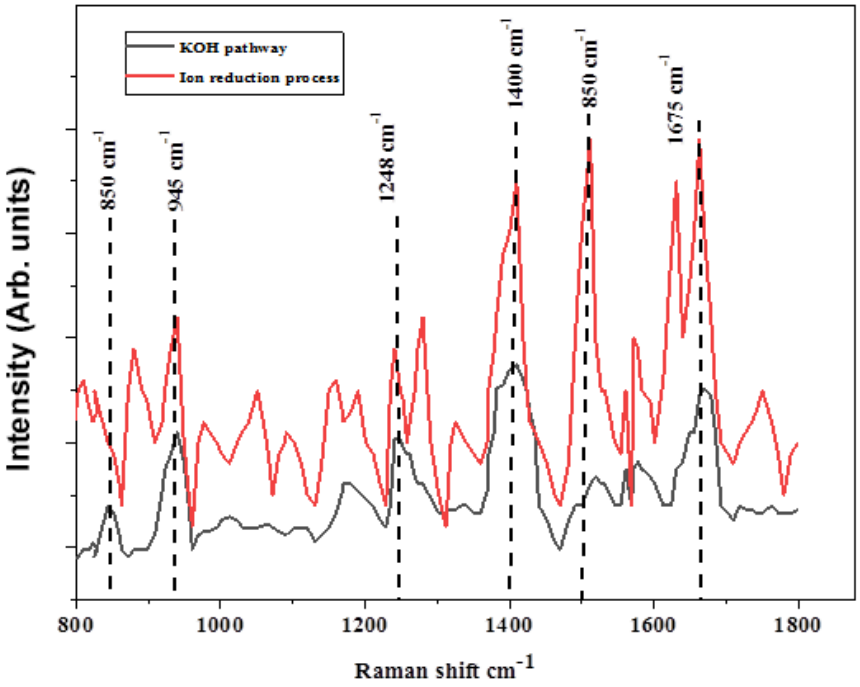

Figure 6: Raman spectrum of as-prepared PSi with 5×10^{-3} M concentration for a) ion reduction process and b) wet chemical KOH method.

As previously stated, the Raman signal was altered, which was attributable to the surface enhancement impact caused by AgNPs deposited on the porous silicon substrate. For the pre-etching ion reduction process, the SERS signal intensity can be seen in **Fig. 7b**. The maximum SERS value of 1.5×10^{4} was achieved when the AgNPs were synthesized using laser intensity of 350 mW/cm^2 and varying concentrations. This value was determined based on the intensity associated with the 1401 cm^{-1} band. Moreover, the phenomenon of Raman enhancement was observed to be particularly significant in samples with higher surface-to-volume ratios, because of the effective transfer of

energy from the local electromagnetic fields to the target molecules. The high relative Raman intensity observed in the SERS substrate is attributed to the reduction in the size of the hotspot regions, which leads to a decrease in the inter-particle distance within these regions.

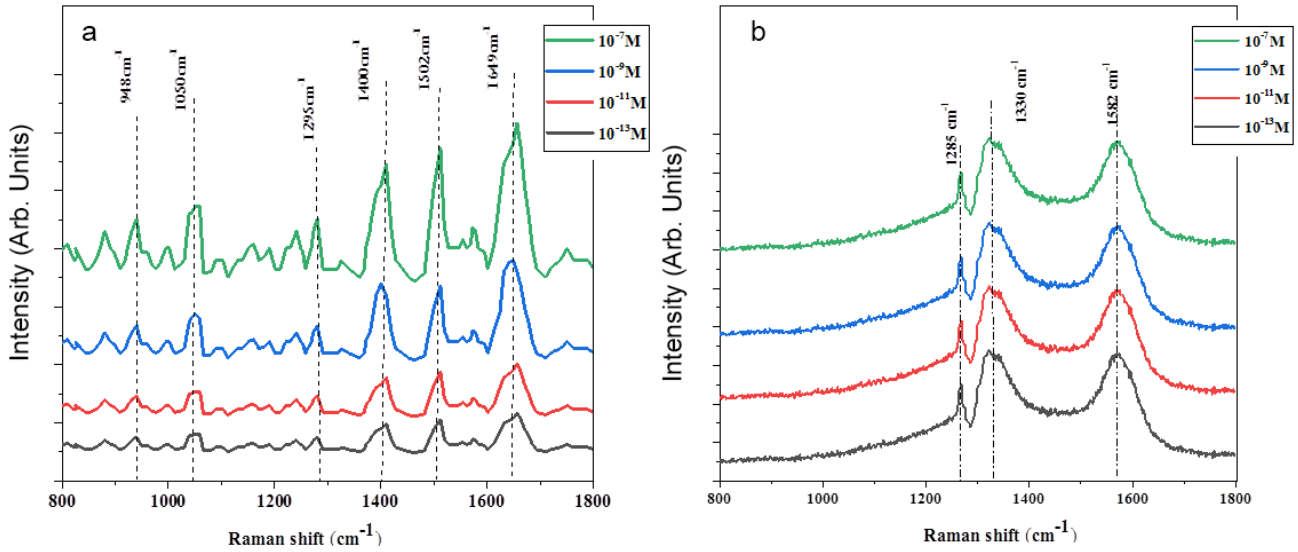

Figure 7: Spectra of SERS for the CIPRO antibiotics/AgNPs/PSi hybrids structures at an intensity of 350 mW/cm^2 and 5×10^{-3}M AgNPs concentrations: (a) pre-etching ion reduction process and (b) KOH method.

Silver particles with smaller sizes can easily penetrate the pores of the silicon. When the surface is exposed to Raman rays, part of the light will be reflected and another part will be absorbed into the pores where internal reflections enhance the signal leading to magnification; thus, amplified rays emerge in addition to the reflected rays on the surface. Raman images proved that the nanoparticles expanded and completely covered the surface, in contrast to the KOH method.

The EF, used to evaluate the lower detection limit, was calculated using **Eq. (2)** as presented below [37]:

$$\boldsymbol{EF = (I_{SERS} \times C_R) / (I_R \times C_{SERS})} \quad \textbf{(2)}$$

Where (I_{SERS} and I_R) denote the SERS signal intensity at the antibiotic molecule concentration C_{SERS}, and the Raman signal intensity at concentration C_R respectively. **Fig. 8** shows the relationship at different processes for the concentration of C_{IPRO} antibiotic and the enhancement factor (EF) of SERS intensity for CIPRO. The EF amount was altered in line with the contribution of CIPRO in the aqueous solution. It was discovered that the greater EF was equal (6.3×10^{12} and 7.78×10^{10}) at 5×10^{-3}M salt concentration for the pre-etching and KOH processes, respectively. After comparing the results of the Raman examination of the two methods of ion reduction process and KOH, it was found that the EF in detecting the lowest concentrations of the CIPRO antibiotic in the ion reduction process is better, and this attributed to parameters like the size of the nanoparticles as well as the hotspot region and a high surface-to-volume ratio.

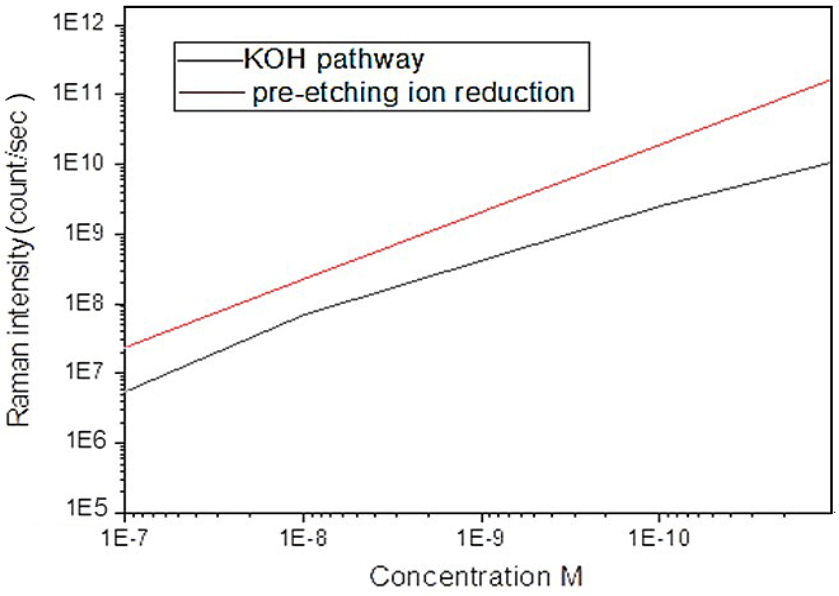

Figure 8: The EF vs. concentration on different methods.

Many factors, such as the highest hotspot region density and LSP, determine the maximal EF. The response mechanism is amplified by smaller AgNPs, which generate a stronger amplified electric field, enabling the detection of even the lowest concentrations of CIPRO antibiotics.

4. Conclusions

In this study, very sensitive chemical sensors were successfully developed that can detect extremely low concentrations of the antibiotic CIPRO. The sensors were prepared using active substrates of AgNPs deposited on PSi. In addition, the methods used in this study were modified to significantly improve their effectiveness. Fixed conditions such as laser intensity and AgNPs concentration were used in the study. The shape of the surface of the nanocrystal-like structure was modified in two different ways: by the ion reduction process before etching and by the KOH method. The shape, the number of holes and the size of the AgNPs/PSi nanocrystals changed, which directly affected their chemical sensing efficiency. The performance of the macro-PSi hybrid structure is closely related to its structural, morphological and optical properties. The topographic layers for the different processes were not completely covered by pores, and the nanoparticles were tiny because there were loose bonds on the substrate. The researchers analyzed the Raman results for both the ion reduction and KOH methods and found that the ion reduction method was more effective in detecting the lowest concentrations of the CIPRO antibiotic. This superiority is attributed to the smaller size of the nanoparticles, the higher density of the hotspots and the higher SSA.

Conflict of Interest

The authors declare that they have no conflict of interest.

References

[1] Z. H. Xiong, S. Yuan, Z. M. Jiang, J. Qin, C. W. Pei, L. S. Liao, *et al.*, "Photoluminescence studies of porous silicon microcavities," *J. Lumin.*, vol. 80, no. 1–4, pp. 137–140, 1998.

[2] P. C. Sharma, A. Jain, S. Jain, R. Pahwa, and M. S. Yar, "Ciprofloxacin: review on developments in synthetic, analytical, and medicinal aspects," *J. Enzyme Inhib. Med. Chem.*, vol. 25, no. 4, pp. 577–589, 2010.

[3] G. G. Zhanel, S. Fontaine, H. Adam, K. Schurek, M. Mayer, A. M. Noreddin, *et al.*, "A review of new fluoroquinolones: focus on their use in respiratory tract infections," *Treat. Respir. Med.*, vol. 5, pp. 437–465, 2006.

[4] K. Ibsen and N. Bhatt, *Review for USMLE: United States Medical Licensing Examination, Step 2 CK*. Lippincott Williams & Wilkins, 2007.

[5] K. Drlica and X. Zhao, "DNA gyrase, topoisomerase IV, and the 4-quinolones," *Microbiol. Mol. Biol. Rev.*,

vol. 61, no. 3, pp. 377–392, 1997.
[6] Y. Pommier, E. Leo, H. Zhang, and C. Marchand, "DNA topoisomerases and their poisoning by anticancer and antibacterial drugs," *Chem. Biol.*, vol. 17, no. 5, pp. 421–433, 2010.
[7] X. Jiang, X. Qin, D. Yin, M. Gong, L. Yang, B. Zhao, *et al.*, "Rapid monitoring of benzylpenicillin sodium using Raman and surface enhanced Raman spectroscopy," *Spectrochim. Acta Part A Mol. Biomol. Spectrosc.*, vol. 140, pp. 474–478, 2015.
[8] A. S. K. Hashmi and G. J. Hutchings, "Gold catalysis," *Angew. Chemie Int. Ed.*, vol. 45, no. 47, pp. 7896–7936, 2006.
[9] P. C. Pinheiro, S. Fateixa, and T. Trindade, "SERS detection of penicillin G using magnetite decorated with gold nanoparticles," *Magnetochemistry*, vol. 3, no. 4, p. 32, 2017.
[10] U. S. Jensen, A. Muller, C. T. Brandt, N. Frimodt-Møller, A. M. Hammerum, D. L. Monnet *et al.*, "Effect of generics on price and consumption of ciprofloxacin in primary healthcare: the relationship to increasing resistance," *J. Antimicrob. Chemother.*, vol. 65, no. 6, pp. 1286–1291, 2010.
[11] A. M. Alwan, A. A. Youssef, and A. A. Chasb, "Controllable synthesization of Au nanoparticles by laser enhanced wet KOH etching process," in *Journal of Physics: Conference Series*, IOP Publishing, 2021, p. 12009.
[12] X. Guo, S. Xu, L. Zhao, W. Lu, F. Zhang, D. G. Evans, *et al.*, "One-step hydrothermal crystallization of a layered double hydroxide/alumina bilayer film on aluminum and its corrosion resistance properties," *Langmuir*, vol. 25, no. 17, pp. 9894–9897, 2009.
[13] J. Wang, D. Li, Q. Liu, X. Yin, Y. Zhang, X. Jing, *et al.*, "Fabrication of hydrophobic surface with hierarchical structure on Mg alloy and its corrosion resistance," *Electrochim. Acta*, vol. 55, no. 22, pp. 6897–6906, 2010.
[14] L. Li, Y. Zhang, J. Lei, J. He, R. Lv, N. Li, *et al.*, "A facile approach to fabricate superhydrophobic Zn surface and its effect on corrosion resistance," *Corros. Sci.*, vol. 85, pp. 174–182, 2014.
[15] J. Ou, W. Hu, M. Xue, F. Wang, and W. Li, "Superhydrophobic surfaces on light alloy substrates fabricated by a versatile process and their corrosion protection," *ACS Appl. Mater. Interfaces*, vol. 5, no. 8, pp. 3101–3107, 2013.
[16] R. Gao, Q. Liu, J. Wang, X. Zhang, W. Yang, J. Liu, *et al.*, "Fabrication of fibrous szaibelyite with hierarchical structure superhydrophobic coating on AZ31 magnesium alloy for corrosion protection," *Chem. Eng. J.*, vol. 241, pp. 352–359, 2014.
[17] Y. Fan, Z. Chen, J. Liang, Y. Wang, and H. Chen, "Preparation of superhydrophobic films on copper substrate for corrosion protection," *Surf. Coatings Technol.*, vol. 244, pp. 1–8, 2014.
[18] Z. Wang, J. Gong, J. Ma, and J. Xu, "In situ growth of hierarchical boehmite on 2024 aluminum alloy surface as superhydrophobic materials," *RSC Adv.*, vol. 4, no. 28, pp. 14708–14714, 2014.
[19] M. S. Mohammed and R. A. Shlaga, "Illumination effects on the physical properties of porous silicon prepared by PECE," *Appl. Nanosci.*, vol. 8, no. 6, pp. 1279–1283, 2018.
[20] L. A. Wali, K. K. Hasan, and A. M. Alwan, "An investigation of efficient detection of ultra-low concentration of penicillins in milk using AuNPs/PSi hybrid structure," *Plasmonics*, vol. 15, no. 4, pp. 985–993, 2020.
[21] R. A. Shlaga, A. M. Alwan, and M. S. Mohammed, "The role of laser irradiation in the modulation of an efficient mud-like structure as PSi layer for nanophotonic sensors," *J. Mater. Sci. Mater. Electron.*, vol. 34, no. 3, p. 208, 2023.
[22] D. A. Hashim, A. M. Alwan, and M. F. Jawad, "An investigation of Structural Properties of Monometallic (Ag, Pd) and Bimetallic (Ag@ Pd) Nanoparticles Growth on Macro Porous Silicon.," *Int. J. Nanoelectron. Mater.*, vol. 11, no. 4, 2018.
[23] Z. C. Zhai Chen, L. Y. Li YongYu, P. Y. Peng YanKun, and X. T. Xu TianFeng, "Detection of chlorpyrifos in apples using gold nanoparticles based on surface enhanced Raman spectroscopy.," *Int J of Agricultural and Biological Engineering* 2015.
[24] L. Y. Liu YanDe, Z. Y. Zhang YuXiang, W. H. Wang HaiYang, and Y. B. Ye Bing, "Detection of pesticides on navel orange skin by surface-enhanced Raman spectroscopy coupled with Ag nanostructures.," *Int J of Agricultural and Biological Engineering* 2016.
[25] S. Devarajan, B. Vimalan, and S. Sampath, "Phase transfer of Au–Ag alloy nanoparticles from aqueous medium to an organic solvent: effect of aging of surfactant on the formation of Ag-rich alloy compositions," *J. Colloid Interface Sci.*, vol. 278, no. 1, pp. 126–132, 2004.

[26] R. A. Shlaga, A. M. Alwan, and M. S. Mohammed, "Fine controlling of the performance nano-photonic sensors by simple, low cost process," *J. Opt.*, vol. 53, no. 3, pp. 1861–1871, 2024.
[27] I. Zubel, K. Rola, and M. Kramkowska, "The effect of isopropyl alcohol concentration on the etching process of Si-substrates in KOH solutions," *Sensors Actuators A Phys.*, vol. 171, no. 2, pp. 436–445, 2011.
[28] M. A. Gosálvez, Y. Xing, and K. Sato, "Analytical solution of the continuous cellular automaton for anisotropic etching," *J. microelectromechanical Syst.*, vol. 17, no. 2, pp. 410–431, 2008.
[29] A. A. Khalaf, A. H. Attallah, A. B. Dheyab, and A. M. Alwan, "Influence of magnetic field on the characteristics of n-type PSi prepared by photo-electro-chemical etching process," in *Journal of physics: Conference series*, IOP Publishing, 2021, p. 12015.
[30] R. B. Rashid, A. B. Dheyab, and A. M. Alwan, "Enhancing the performance of p_n junction Si solar cells by integrating silver core&gold shell nano-particles," *Opt. Quantum Electron.*, vol. 54, pp. 1–10, 2022.
[31] R. B. Rashid, A. M. Alwan, and M. S. Mohammed, "Improved Difenoconazole pesticide detection limit via double-sided porous silicon layers' electrical sensor," *Mater. Chem. Phys.*, vol. 293, p. 126898, 2023.
[32] A. B. Dheyab, "Study of the influence of incorporation of gold nanoparticles on the modified porous silicon sensor for petroleum gas detection," *Eng. Technol. J.*, vol. 35, no. 8 Part A, 2017.
[33] A. M. Alwan, A. A. Yousif, and L. A. Wali, "The growth of the silver nanoparticles on the mesoporous silicon and macroporous silicon: a comparative study," 2017.
[34] Y. Chao, Q. Zhou, Y. Li, Y. Yan, Y. Wu, and J. Zheng, "Potential dependent surface-enhanced Raman scattering of 4-mercaptopyridine on electrochemically roughened silver electrodes," *J. Phys. Chem. C*, vol. 111, no. 45, pp. 16990–16995, 2007.
[35] S. A. Maier, *Plasmonics: fundamentals and applications*, vol. 1. Springer, 2007.
[36] S. Schlücker, "Surface-Enhanced raman spectroscopy: Concepts and chemical applications," *Angew. Chemie Int. Ed.*, vol. 53, no. 19, pp. 4756–4795, 2014.
[37] R. A. Ismail, K. S. Khashan, and A. M. Alwan, "Study of the effect of incorporation of CdS nanoparticles on the porous silicon photodetector," *Silicon*, vol. 9, pp. 321–326, 2017.